Thin Solid Films 519 (2010) 7382–7385

Contents lists available at ScienceDirect

Thin Solid Films

journal homepage: www.elsevier.com/locate/tsf

Cu_2ZnSnS_4 solar cells prepared with sulphurized dc-sputtered stacked metallic precursors

P.A. Fernandes [a,b,*], P.M.P. Salomé [a], A.F. da Cunha [a], Björn-Arvid Schubert [c]

[a] I3N-Departamento de Física, Universidade de Aveiro, Campus Universitário de Santiago, 3810-193 Aveiro, Portugal
[b] Departamento de Física, Instituto Superior de Engenharia do Porto, Instituto Politécnico do Porto, Rua Dr. António Bernardino de Almeida, 431, 4200-072 Porto, Portugal
[c] Helmholtz-Zentrum Berlin für Materialien und Energie GmbH Solarenergieforschung, Hahn-Meitner-Platz 1, 14109 Berlin, Germany

ARTICLE INFO

Available online 17 December 2010

Keywords:
Cu_2ZnSnS_4
CZTS
Sputtering
Sulphurization
Thin film
Solar cell
Raman

ABSTRACT

In the present work we report the details of the preparation and characterization results of Cu_2ZnSnS_4 (CZTS) based solar cells. The CZTS absorber was obtained by sulphurization of dc magnetron sputtered Zn/Sn/Cu precursor layers. The morphology, composition and structure of the absorber layer were studied by scanning electron microscopy, energy dispersive spectroscopy, X-ray diffraction and Raman scattering. The majority carrier type was identified via a hot point probe analysis. The hole density, space charge region width and band gap energy were estimated from the external quantum efficiency measurements. A MoS_2 layer that formed during the sulphurization process was also identified and analyzed in this work. The solar cells had the following structure: soda lime glass/Mo/CZTS/CdS/i-ZnO/ZnO:Al/Al grid. The best solar cell showed an open-circuit voltage of 345 mV, a short-circuit current density of 4.42 mA/cm^2, a fill factor of 44.29% and an efficiency of 0.68% under illumination in simulated standard test conditions: AM 1.5 and 100 mW/cm^2.

1. Introduction

Research is currently in progress to develop thin film solar cells that are not based on scarce elements, like In and Ga elements, and toxic elements, like Se. The replacement of the successful $CuIn_{1-x}Ga_xSe_2$ (CIGS) absorber, that leads to cells with efficiency around 20% [1], has proved to be a difficult task. One of the most promising candidates is the Cu_2ZnSnS_4 (CZTS) compound. Despite the increase in the number of research groups that claim to have achieved successful growth of this semiconductor compound, only a few presented results of complete solar cells.

The methods tested so far to grow this compound can be classified into two main categories: vacuum and non-vacuum techniques. Both categories use similar growth schemes, that is, they comprise deposition of the precursors and annealing in a sulphur vapour atmosphere or in a H_2S atmosphere. Katagiri et al. [2], using a vacuum growth method, namely rf-magnetron co-sputtering technique of Cu, SnS, and ZnS for the deposition of the precursors and a sulphurization process using H_2S atmosphere, made a solar cell that reached a conversion efficiency of 6.7%. For non vacuum techniques the highest solar cell efficiency, 3.4%, was attained by Ennaoui et al. [3]. This method used co-electroplated metal precursors followed by a solid state reaction in a H_2S atmosphere. In the present work we report the details of the preparation and characterization results of CZTS based solar cells. The CZTS absorber was obtained by sulphurization of dc magnetron sputtered Zn/Sn/Cu precursors.

2. Experimental details

2.1. Sample preparation

The sample preparation followed the same procedure described in previous works [4]. The deposition order of the metallic precursors was Zn/Sn/Cu. The CZTS formation was performed in a tubular furnace in a N_2 and sulphur vapour atmosphere at a constant working pressure of 5.6×10^{-1} mbar and a N_2 flow rate of 40 ml min^{-1}. The sample was sulphurized at a maximum temperature of 525 °C for 10 min. After the sulphurization process a KCN chemical treatment was applied to remove $Cu_{2-x}S$ spurious phases.

To prepare a solar cell the following step was the deposition of n-type CdS by dipping the samples in a chemical bath. The process allows the formation of a heterojunction with the p-type CZTS. Next a ZnO/ZnO:Al window layer was deposited by RF-magnetron sputtering. Finally, Ni/Al metal grids were deposited by e-beam evaporation through an aperture mask to form the front contact.

2.2. Characterization

The thickness of the metallic precursors was monitored in situ using a quartz crystal monitor. X-ray diffraction analysis (XRD) was

* Corresponding author. I3N-Departamento de Física, Universidade de Aveiro, Campus Universitário de Santiago, 3810-193 Aveiro, Portugal.
E-mail addresses: pafernandes@ua.pt (P.A. Fernandes), psalome@ua.pt (P.M.P. Salomé), antonio.cunha@ua.pt (A.F. da Cunha), bjoern.schubert@helmholtz-berlin.de (B.-A. Schubert).

0040-6090/$ – see front matter © 2010 Elsevier B.V. All rights reserved.
doi:10.1016/j.tsf.2010.12.035

performed with a PHILIPS PW 3710 system equipped with a Cu-Kα source (wavelength λ = 1.54060 Å) and the generator settings were 50 mA and 40 kV. A Hitachi S4100 scanning electron microscopy (SEM) and a Rontec energy dispersive spectroscopy (EDS) with setting parameters of 25 kV and 10 μA were used for morphological and compositional analyses. The composition of the precursors was performed by inductively coupled plasma mass spectrometry (ICP-MS) using an ICP-MS Thermo X Series. Raman scattering measurements were performed at room temperature in the backscattering configuration and the excitation laser line used was 488 nm. The Jobin-Yvon T64000 Raman spectrometer was equipped with an Olympus microscope with a 100× magnification lens. Current–voltage characteristics of the solar cells were measured under illumination in simulated standard test conditions: AM1.5 and 1000 W/m^2. External quantum efficiency (EQE) measurements were performed by a two source illumination system (xenon and halogen lamp) combined with a monochromator (BENTHAM TM300). A calibrated Si-cell was used as reference for the $J(V)$ as well as for the EQE measurements. The majority carrier type was identified using a hot point probe device.

For the absorber's back surface measurements, a carbon conductive tape was used to detach the film from the substrate.

3. Results and discussion

3.1. Compositional characterization

Table 1 shows the results of the compositional analysis for precursors, and top and bottom CZTS surfaces. The ICP-MS technique was used for the precursors' analysis and EDS for the CZTS compound. Samples with a layered structure are not suitable for compositional analysis through EDS. Its interaction volume and limited penetration depth are the reasons of an overestimation of top layers. The results in Table 1 show that the inter-diffusion in the absorber layer was not completed, and non uniform distribution of the metallic elements remains after the sulphurization process. It can also be noted that precursors are Cu poor and Zn rich.

3.2. Structural characterization

Structural characterization was done using two techniques, XRD and Raman scattering. Fig. 1 shows the results for XRD analysis. The phase identification pointed to the presence of CZTS with the kesterite structure and Mo, according to the International Centre for Diffraction Data (ICDD) [5]. The XRD pattern also shows sharp peaks that indicate good crystallinity.

Fig. 2a) shows the Raman scattering pattern for the top view of the CZTS layer. It shows the main CZTS peaks at 288 cm^{-1}, 338 cm^{-1} and 368 cm^{-1}, which are in agreement with the literature [6,7]. Due to the limited penetration depth of the Raman scattering technique, the back side of the CZTS layer was also analyzed. The results are presented in Fig. 2b). This figure shows four sharp peaks at 288 cm^{-1}, 338 cm^{-1}, 383 cm^{-1} and 408 cm^{-1}, and a broad peak at 454 cm^{-1}. According to Jiménez Sandoval et al. [8], all these peaks are attributable to the MoS_2 compound, except the peak at 338 cm^{-1} which belongs to CZTS. The peak at 288 cm^{-1} is common to the CZTS and MoS_2 compounds. Note that the measurement conditions for the front and back sides of the absorber layer were kept constant.

Table 1
Composition ratios for metallic precursor layers and CZTS.

	$\frac{[Cu]}{[Zn]+[Sn]}$	$\frac{[Zn]}{[Sn]}$	$\frac{[Cu]}{[Zn]}$	$\frac{[Cu]}{[Sn]}$	Method
Precursors	0.9	1.4	1.5	2.2	ICP-MS
CZTS (top)	0.9	1.4	1.6	2.2	EDS
CZTS (bottom)	0.6	2.3	0.9	1.9	EDS

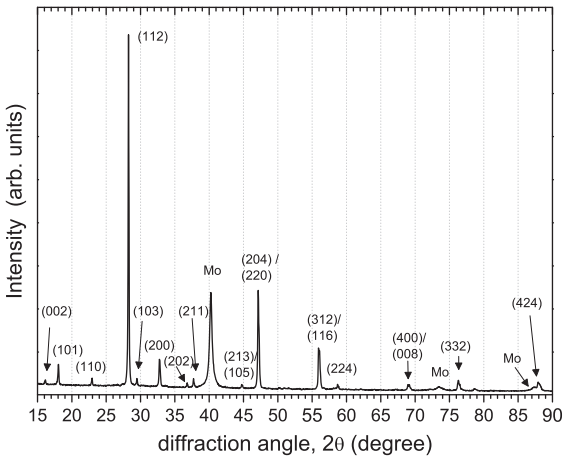

Fig. 1. XRD diffractogram of the CZTS layer.

3.3. Morphological characterization

Fig. 3a) shows a SEM micrograph of the surface of the absorber layer. It shows that the film is compact but presents some roughness. This figure also shows that this layer is composed of small grains. Fig. 3b) shows the morphology of the MoS_2 layer. This layer formed during the sulphurization process presents an irregular surface probably due to the peeling process. In Fig. 4 is presented the cross sectional SEM of the CZTS layer. Again, this micrograph shows an absorber layer composed of a compact film with small grains. Between the CZTS layer and the Mo back contact, a layer with a thickness of around 500 nm, which corresponds to MoS_2, is observed. This thickness is high when compared with the value reported in the literature [9]. Voids can also be seen between the MoS_2 and the CZTS layer, which can constitute a problem for the solar cell performance.

3.4. Electrical characterization

Solar cells with a total area of 0.5 cm^2 were prepared and characterized. Generally all cell parameters were low. In Fig. 5 the J–V characteristics of the best solar cell are presented. The performance parameters were: short circuit current density, j_{sc}, 4.42 mA/cm^2, open circuit voltage, V_{oc}, 345 mV, fill factor, FF, 44.3% and conversion efficiency, η, 0.68% under simulated AM1.5 illumination. Shunt and series resistances, R_{sh} and R_s, were 517 Ω and 5.6 Ω, respectively. Comparing the various cells made from the same sample some fluctuation in the

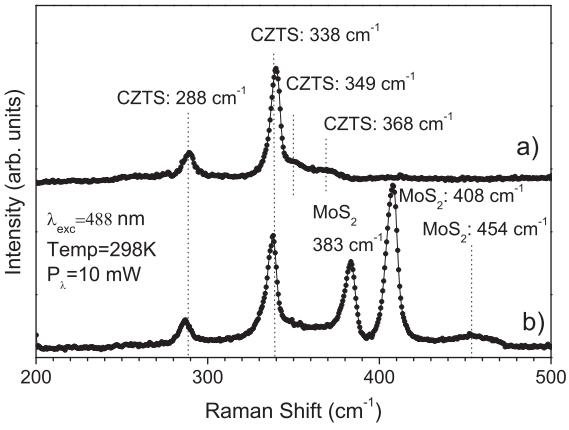

Fig. 2. Raman scattering spectra of the absorber layer: a) front side of the absorber layer and b) back side of the absorber layer.

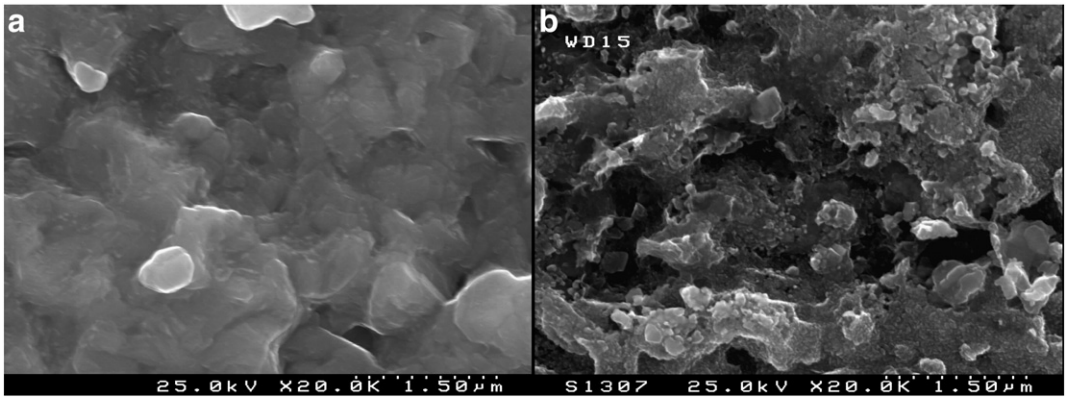

Fig. 3. SEM micrograph of the CZTS surface. Despite presenting a compact film this sample presents some roughness. b) SEM micrograph of the back side of the CZTS layer. The irregular surface corresponds to MoS_2.

electrical parameters was observed. This means that the sample was inhomogeneous and therefore further adjustments of the growth process are required.

The EQE of the best cell and the absorption coefficient of the CZTS layer are shown in Fig. 6. The EQE shows a low overall spectral response indicating a high recombination rate. The low energy side of the EQE spectrum presents some important features which are related to the absorber layer properties. For wavelengths higher than 500 nm, the curve decays with two different slopes. The first between 500 nm and 700 nm is believed to be due to the low diffusion length of the minority carriers in the CZTS layer and the second, steeper one, corresponds to the absorption threshold which is reached when the incident photon energy equals the CZTS band gap energy. Even though they may be present at residual level, the spurious phases, namely cubic-Cu_2SnS_3 which have lower band gap energy [10], may account for part of the high recombination present in the cells. Fig. 6 also shows the absorption coefficient spectrum of the CZTS estimated from the transmittance and reflectance measurements; the method is described elsewhere [10].

The results of EQE analysis are used in Fig. 7a), which shows the $h\nu \cdot \ln(1-EQE)^2$ vs photon energy graph, for the estimation of the energy band gap. The value obtained, 1.65 eV, is higher than those values estimated by either using transmittance and reflectance measurements, 1.50 eV [10] or those by diffuse reflectance, 1.43 eV [4]. Fig. 7b) presents $\ln(1-EQE)^2$ vs the absorption coefficient and its linear data fitting which permits the estimation of the space charge region width, W_D, according to the work done by Scragg et al. [11]. The value obtained for the space charge region width was 60 nm which is low compared with the values already published for CZTS, 340 nm and 190 nm [11]. Such low space charge region width is probably consistent with the overall high recombination discussed above since it means that many defects are present in the CZTS. Some of the defects are actually doping the material and we expect high doping densities which in turn lead to a low space charge region width. Using that value, considering the built-in potential parameter in thermal equilibrium for an abrupt junction $\psi_{bi} - \frac{2KT}{q} = 0.5\,V$, and considering the relative permittivity of CZTS, ε_S, identical to that of $CuInS_2$ hence equal to 10, in equation [12]:

$$N = \frac{2\varepsilon_s}{qW_D^2}\left(\psi_{bi} - \frac{2KT}{q}\right) \quad (1)$$

we estimate a value for the carrier concentration, N, of $1.5\times10^{17}\ cm^{-3}$. This value is higher than those reported for either the CZTS [11] or CIGS [13], but close to the values reported for CZTS grown by the same method [4], using C–V measurements for its estimation.

4. Conclusions

In this work we present and discuss the performance results of a thin film solar cell in which the CZTS absorber was grown from stacked dc sputtered metallic precursors. The best solar cell had an efficiency of 0.68% which is rather low despite the fact that XRD and Raman analyses point to good CZTS crystallinity and the absence of spurious phases.

The CZTS top and bottom side compositional analysis, by EDS, indicates a high concentration of Zn at the bottom while at the top

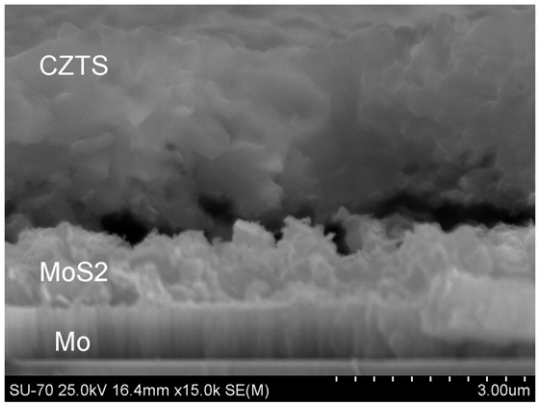

Fig. 4. Cross sectional SEM micrograph of the SLG/Mo/CZTS films. A MoS_2 layer has been identified between the Mo back-contact and the CZTS layer.

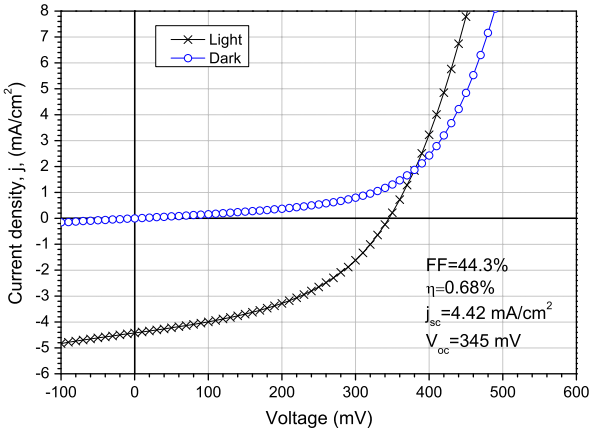

Fig. 5. J–V characteristics of the best solar cell.

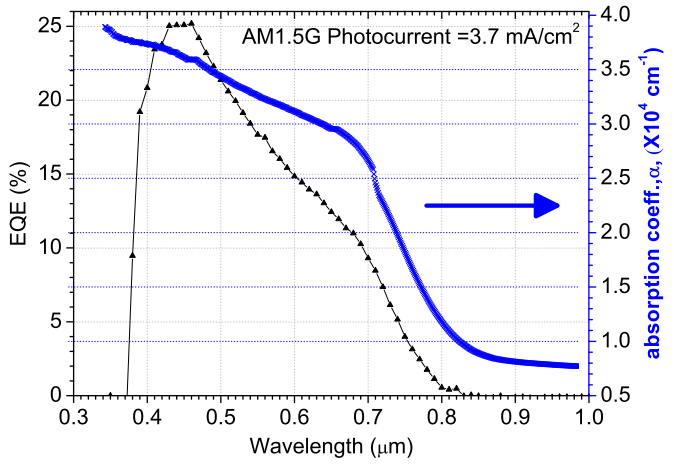

Fig. 6. EQE spectrum of the best solar cell and absorption coefficient spectrum of the corresponding CZTS absorber layer.

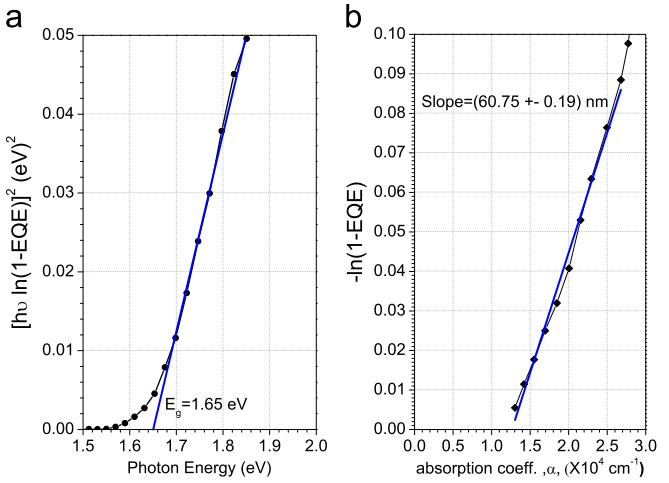

Fig. 7. a) $h\nu \cdot \ln(1-EQE)^2$ vs photon energy and the estimation of the band gap of Cu_2ZnSnS_4 films. b) $\ln(1-EQE)^2$ vs the absorption coefficient and space charge region width estimation.

the composition is very close to that of the precursors. This compositional depth non-uniformity is likely to give rise to the formation of a high defect density leading to increased recombination. Furthermore the structural and morphological analyses performed on the bottom side of the absorber layer showed the presence of a MoS_2 layer which is formed during the sulphurization process. The effect on the cell performance of this layer is not known.

The EQE analysis led to a rather low space charge region width and a carrier concentration which are consistent results.

To improve the cell performance we believe that it is necessary to improve depth composition uniformity which can, perhaps, be achieved by either increasing the sulphurization time allowing for a better diffusion of the elements during the annealing process or reducing the thickness of the absorber layer. Passivating, somehow, some of the CZTS intrinsic defects may be useful to reduce the recombination hence enhancing the cell performance.

Acknowledgments

P.A. Fernandes acknowledges the financial support of the Fundação para a Ciência e Tecnologia (FCT), through a PhD grant number SFRH/BD/49220/2008. P.M.P. Salomé acknowledges the financial support of FCT, through a PhD grant number SFRH/BD/29881/2006. FCT is also acknowledged for the financial support of the national electronic microscopy network, whose services we have used, through the grant REDE/1509/RME/2005.

References

[1] Ingrid Repins, M. Contreras, B. Egaas, C. DeHart, J. Scharf, C. Perkins, B. To, R. Noufi, Prog. Photovoltaics 16 (2008) 235.
[2] H. Katagiri, K. Jimbo, S. Yamada, T. Kamimura, W.S. Maw, T. Fukano, T. Ito, T. Motohiro, Appl. Phys. Exp. 1 (2008) 041201.
[3] A. Ennaoui, M. Lux-Steiner, A. Weber, D. Abou-Ras, I. Kötschau, H.-W. Schock, R. Schurr, A. Hölzing, S. Jost, R. Hock, T. Voβ, J. Schulze, A. Kirbs, Thin Solid Films 517 (2009) 2511.
[4] P.A. Fernandes, P.M.P. Salomé, A.F. da Cunha, Semicond. Sci. Technol. 24 (2009) 105013.
[5] International Centre for Diffraction Data — Ref. Code, 01-075-4122 (Cu_2ZnSnS_4), 04-003-2919 (Mo).
[6] P.A. Fernandes, P.M.P. Salomé, A.F. da Cunha, Thin Solid Films 517 (2009) 2519.
[7] M. Altosaar, J. Raudoja, K. Timmo, M. Danilson, M. Grossberg, J. Krustok, E. Mellikov, Phys. Status Solidi A 205 (2008) 167.
[8] S. Jiménez Sandoval, D. Yang, R.F. Frindt, J.C. Irwin, Phys. Rev. B 44 (1991) 3955.
[9] Jonathan J. Scragg, Dominik M. Berg, Phillip J. Dale, J. Electroanal. Chem. 646 (2010) 52.
[10] P.A. Fernandes, P.M.P. Salomé, A.F. da Cunha, Phys. Status Solidi C 7 (2010) 901.
[11] Jonathan J. Scragg, Phillip J. Dale, Laurence M. Peter, Electrochem. Commun. 10 (2008) 639.
[12] S.M. Sze, Knok K. Ng, "Physics of Semiconductor Devices", 3rd Edition, Wiley-Interscience, Chap 2, pp 83.
[13] D. Lincot, H.G. Meier, J. Kessler, J. Vedel, B. Dimmler, H.W. Schock, Sol. Energy Mater. 20 (1990) 67.